Anomalous photoemission from Ag(100) in the femtosecond regime

GianPiero Banfi,[1] Gabriele Ferrini,[2] Marco Peloi,[2] and Fulvio Parmigiani[2]
[1]*Istituto Nazionale per la Fisica della Materia and Dipartimento di Elettronica, Università di Pavia, I-27100 Pavia, Italy*
[2]*Istituto Nazionale per la Fisica della Materia and Dipartimento di Matematica e Fisica, Università Cattolica, I-25121 Brescia, Italy*
(Received 6 August 2002; published 31 January 2003)

We investigate the nonlinear photoemission from a silver monocrystal with femtosecond laser pulses in a wide range of photon energies ($0.8\ \text{eV} < h\nu < 6.3\ \text{eV}$). Electrons with high kinetic energy are observed in all cases of nonlinear photoemission and at intensities much smaller than 1 GW/cm^2. In the infrared, the electron distribution resembles a decreasing exponential, the tail extending up to tens of eV. At $h\nu = 3.1$ eV such exponential distribution coexists with the Fermi-Dirac distribution due to two-photon emission. An explanation in terms of nanosize protuberancies, heated by localized surface plasmons cannot be ruled out, but alternative pictures, however speculative, are worth being considered.

DOI: 10.1103/PhysRevB.67.035428 PACS number(s): 71.10.Ca, 79.60.Bm

I. INTRODUCTION

Nonlinear photoemission from metals irradiated with high peak power laser pulses has been investigated as soon as picosecond and femtosecond lasers were available.[1–4] Pulses of short time duration are ideal to study the electronic behavior since they allow to employ high intensity without heating the lattice. Early measurements concentrated on the power dependence of the yield versus pulse energy and evidenced that it changes according to the intensity regime. Bloembergen and co-workers explained this complex power dependence by introducing the concept of thermally assisted photoemission.[2–4] In the last decade two photon photoemission (2PPE) attracted interest as a fundamental tool in the study of the lifetime and dephasing time of surface states,[5–8] and has also proved to be a promising technique for the study of adsorbates.[9–11]

In this paper we present results on an intriguing aspect associated to photoemission with short pulses which is not yet properly understood and also poorly characterized. In fact, irradiation of metals with photons of energy $h\nu$ smaller than the work function W, may lead to the generation of electrons with a kinetic energy up to several $h\nu$, and with a spectrum without the discrete steps expected for a multiphoton absorption. This behavior can be observed even at moderate intensities, as we shall show.

High kinetic energy electron photoemission was first observed with picosecond pulses, a regime where the interpretation can be even more difficult.[12–15] Using femtosecond pulses, the authors of Ref. 16 reported for copper the expected one-photon and two-photon spectra (with a sharp cutoff on the high kinetic energy side) when the photon energy was 4.5 and 3 eV, respectively. They still found photoemission at $h\nu \approx 1.5$ eV, but with a featureless spectrum and an electron kinetic energy (KE) extending up to 6–8 eV. In this case, they attributed the emission to a process similar to tunnel ionization in atoms. Since tunnel ionization requires fields much higher than those of the laser pulse, they proposed a field enhancement mechanism similar to the one invoked in ''surface enhanced Raman scattering'' or in ''enhanced second harmonic generation,'' namely, surface plasmons excited by the laser pulse through surface roughness. Also the high kinetic energy part of the spectrum could be attributed to the field associated to surface plasmons: this field would accelerate the electrons once in vacuum through the ponderomotive force. Indeed kinetic energies of tens and even hundreds of eV have been recently measured with arrangements specifically chosen and designed to couple the laser pulse to a surface plasmon, such as total internal reflection at the prism-metal film interface[17] or the regular surface modulation produced by a grating.[18]

Here we investigate the nonlinear photoemission from a silver monocrystal using a broad range of wavelengths: beside the fundamental pulse from a femtosecond Ti-sapphire laser and its harmonics, we also employed pulses down converted in the infrared ($h\nu = 0.8$ eV). In principle, an infrared (IR) excitation is appropriate to discriminate between multiphoton processes and those mechanism—tunneling and acceleration included—which benefit from a large quiver velocity. To characterize the surface, we used two-photon photoemission from image states, taking advantage of the specific information offered by this nonlinear process.

High kinetic energy electrons (hot electrons) are observed in all cases of nonlinear photoemission and at intensities much smaller than 1 GW/cm^2. Common signature at the different photon energies are a yield which scales approximately with the third power of the intensity, independently of $h\nu$, and a shape of the electron spectrum similar to a Maxwell-Boltzmann distribution, with the high-energy tail extending up to tens of eV. On excitation with the Ti:Sapphire second harmonic, the photoemission shows the coexistence of two distributions: a hot electron distribution appears on top of the Fermi-Dirac distribution and becomes more relevant at increasing intensities. Various mechanisms will be considered to explain photoemission in the IR and the presence of hot electrons. Multiphoton emission can be ruled out, as well as tunneling photoemission and electron acceleration promoted by surface plasmons. A more realistic picture is that of localized-plasmons assisted electron heating at surface imperfections to temperatures close to 0.5 eV, from which thermal emission follows. Some speculative scenarios will be also mentioned, legitimated in so doing by the diffi-

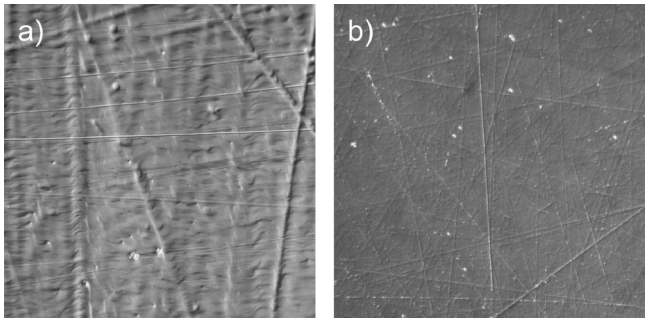

FIG. 1. Atomic force microscope images of the surfaces of the samples. (a) Sample No. 1. (b) Sample No. 2. In both figures the size of the area is 120×120 μm^2.

culty to find a convincing explanation within more conventional processes. Finally, we notice that the above features of nonlinear photoemission could be exploited to produce a bursts of energetic electrons[19,20] and that, in addition to more fundamental motivations, the study of hot electrons at metal surfaces and the efforts to clarify the physical mechanism responsible for them can be of relevance in the field of photocatalysis.

The paper is organized as follows. In Sec. II we report the experimental arrangement and in Sec. III the results. Discussion follows in Sec. IV , while Sec. V is dedicated to surface plasmon and roughness. The conclusions are summarized in Sec. VI.

II. THE EXPERIMENTAL SETUP

The measurements are performed on an Ag(100) single crystal, $8\times8\times2$ mm^3 in size, oriented within an error of ±2 °. The surface is polished with standard optical methods. The experiments are carried out in an ultrahigh vacuum system at a base pressure better than 5×10^{-10} mbar at room temperature. The first sample (sample No. 1) is cleaned by two cycles of Ar sputtering and annealing at about 800 K. The surface quality is tested by means of low-energy electron diffraction (LEED) and Auger spectroscopy. No contaminants are detected, within the Auger sensitivity and the expected LEED image is observed. After the measurements, the sample was extracted from the vacuum chamber and analyzed by atomic force microscopy (AFM) in air. We denote by $\boldsymbol{\rho}$ a vector that span the plane of the surface and by z a coordinate normal to it; by $h(\boldsymbol{\rho})$ the height profile of the interface between metal and vacuum as a function of $\boldsymbol{\rho}$ and by $h_{\mathbf{q}}$ its spatial transform. The root mean square of the height profile is indicated with $h_{\text{r.m.s.}}$. Different spots, randomly chosen, exhibit a similar roughness, with $h_{\text{r.m.s.}}=12$ nm. The height profile of a 120×120 μm^2 spot is shown in Fig. 1. The power spectrum is rather flat, with $\langle|h_{\mathbf{q}}|^2\rangle$ changing by less than a factor of 2 in the region of q's comparable to the wavevector of the light ($q/2\pi=0.6-2.5$ μm^{-1}). Some measurements have been performed on a second sample (sample No. 2) which was prepared with the purpose to test a possible dependence of the feature of photoemission on the roughness of the surface. The surface of sample No. 2 underwent a more accurate optical polishing and, once in the chamber, it was exposed to a softer cleaning procedure consisting of five cycles of sputtering and annealing at 600 K. Its height profile from AFM is also shown in Fig. 1 and one can easily appreciate the difference with sample No. 1. Indeed sample No. 2 shows $h_{\text{r.m.s.}}=3-4$ nm, and a quite smooth power spectrum.

Femtosecond pulses ($\tau_p\approx150$ fs, τ_p is the pulse temporal width) at a fundamental wavelength of 0.79 μm ($h\nu=1.57$ eV) are obtained from a regenerative Ti-sapphire laser system operated at 1 kHz repetition rate. Second harmonic ($h\nu=3.14$ eV) and fourth harmonic ($h\nu=6.28$ eV) are generated through thin β-barium-borate (BBO) crystals, while tunable ultrashort pulses are obtained from the fundamental with a traveling-wave optical parametric generator (TOPG), based on BBO in type II phase matching. The signal wave of the TOPG ($h\nu=0.77-1.03$ eV), together with its harmonics, allows to obtain light pulses at various frequencies as required in the experiment. A long focal lens ($f=4$ m) gently focuses the beam and produces a smooth intensity pattern in the focal plane, where the sample is positioned. The intensity pattern is detected with a charged coupled device (CCD) camera and/or a knife-edge measurement performed in an equivalent position in air. Dimensions and spot sizes reported in the following are taken at the full width at half maximum (FWHM) of the fluence. The diameter of the illuminated area is typically 0.7–1 mm.

The sample is mounted on a sample holder connected with a ultra highvacuum manipulator with five degrees of freedom. The sample holder is isolated from the chamber, so that it can be either grounded or connected to a picoammeter in order to measure the total photocurrent.

The kinetic energy of the photoemitted electrons is measured by a time of flight (TOF) spectrometer. Completely shielded from the external magnetic fields, the TOF spectrometer is mounted in the μ-metal experimental chamber. The residual magnetic field inside the experimental chamber and in the TOF spectrometer is smaller than 10 mG. The TOF parameters have been optimised by electrons trajectories simulations. After drifting through a 445 mm long field free region, the photoelectrons are accelerated onto a pair of multichannel plates and the time of flight is recorded by a multihit time-to-amplitude converter. The active area of the multichannel plate is 1200 mm^2, resulting in a geometrical acceptance angle of $\pm$ 2.6 °. The overall electronic noise of the system is less than 10^{-2} counts/sec and the energy resolution is expected to be better than 30 meV (at KE $=2$ eV). The angle between b (the direction of the impinging optical beam) and t (the TOF axis) is fixed at 30 °. Measurements have been taken with the sample surface perpendicular either to b or to t.

III. RESULTS

A. Reflectivity

The reflectivity measurements at the fundamental wavelength (790 nm) and the second harmonic (395 nm) are realized collecting the light within a cone with an aperture of 4,° around the specular reflection. Taking into account

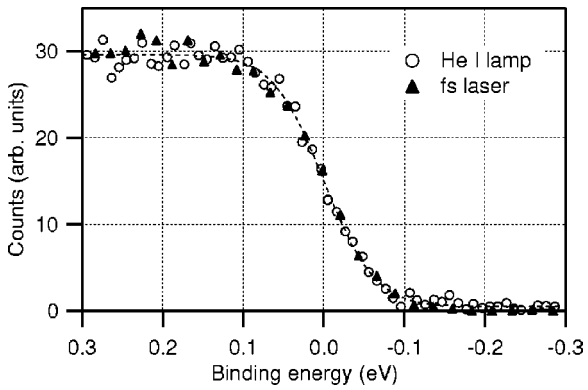

FIG. 2. One photon photoemission spectrum obtained with (▲) 150 fs pulses at $h\nu=6.28$ eV (fourth harmonic of the fundamental) and the time of fligth spectrometer, (○) He I emission line at $h\nu=21$ eV and the hemispherical analyzer. The dashed line represents the best fit of the room-temperature Fermi-Dirac distribution to the data.

Fresnel losses and scattering, we estimate that the lower limits of the Ag sample reflectivity are 0.95 at 790 nm and 0.8 at 395 nm.

B. Linear photoemission

Figure 2 shows the Fermi edge photoemission spectrum excited by the fourth harmonic of the fundamental wavelength. Since the photon energy ($h\nu=6.28$ eV) is larger than the work function W ($W\approx4.6$ eV), the photoemission is linear in this case [one photon photoemission (1PPE)] and the yield is proportional to the pulse energy. The laser Fermi edge spectrum is compared with the Fermi edge detected with an hemispherical analyzer and excited by a He-I emission line at $h\nu=21$ eV. Giving allowance for the obvious translation in energy, the two spectra can be overlapped quite precisely. By fitting the spectrum with the Fermi-Dirac distribution at room temperature, we infer that the energy resolution of TOF spectrometer is better than 0.06 eV.

C. Nonlinear photoemission

Results of the nonlinear photoemission measurements at $\hbar\omega=3.14$ eV are shown in Figs. 3 and 4, those at 1.57 and 0.8 eV in Figs. 5 and 6, respectively. The photoemission geometry is shown in each figure. In the plots reporting the yield [Figs. 3(c), 5(c), 6(c)], the vertical axis shows the photoelectrons collected and detected by the TOF. The collection aperture of TOF is about 10^{-3} strad, and—assuming an isotropic emission—the number of ''counts/sec'' is quite close to the number of ''total electrons emitted per pulse.'' We checked this numerical coincidence to be approximately verified by measuring in a few cases the total photoemitted current. We find that the spectra and the yields are not crucially dependent on the polarization direction and on whether the surface of the sample is normal to *t* or to *b*.

Quite interesting is the situation which is observed by irradiating with the second harmonic pulses (Figs. 3 and 4). The energy of a photon ($h\nu=3.14$ eV) is sufficient to promote 2PPE. Indeed the spectra show a sharp Fermi-edge at a

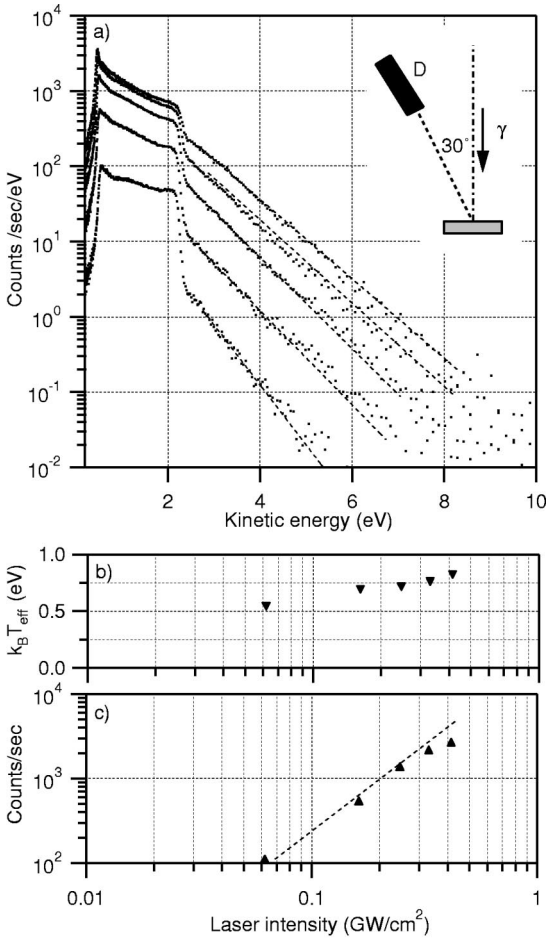

FIG. 3. Irradiation: $h\nu=3.14$ eV, normal incidence. (a) Energy spectra of photoemitted electrons at different intensities. Dashed lines are fits of the exponential function $\exp(-\beta E)$ to the high energy tails. (b) Plot of the ''effective temperature'' (T_{eff}) versus intensity. Irradiated area: 0.9 mm^2. (c) Integrated electron yield versus intensity. Each point is obtained from the energy integration of the spectra reported in (a). The dashed line represent a second order power dependence on intensity.

KE corresponding to $2h\nu-W$. Moreover, at larger kinetic energy, a hot electron tail is evidenced. The number of the electrons collected per pulse increase as I^2 when integrated over the spectrum, while the number of hot electrons, i.e., those photoemitted with KE$>$2eV, has an intensity dependence close to I^3.

With both infrared radiations (see Figs. 5 and 6) the yield grows approximately as I^3 (where I is the peak intensity) before saturation. The spectrum resembles a decreasing exponential, with a behavior similar to the hot electron tail observed in the second harmonic spectra. At $h\nu=0.8$ eV and at $I\approx1$ GW/cm^2, we estimate that each pulse photoemits about 10^4 electrons/cm^2 with KE$>$10 eV.

A Maxwell-Boltzmann distribution is fitted to the hot electron spectra and the hot electron population ic characterized with its temperature T_{eff}. The values of T_{eff} are reported in Figs. 3, 5, 6. We find that for excitation in the visible $T_{\text{eff}}\approx0.6-0.8$ eV, depending on the intensity. The equivalent temperature increases to over 2 eV with photon energy

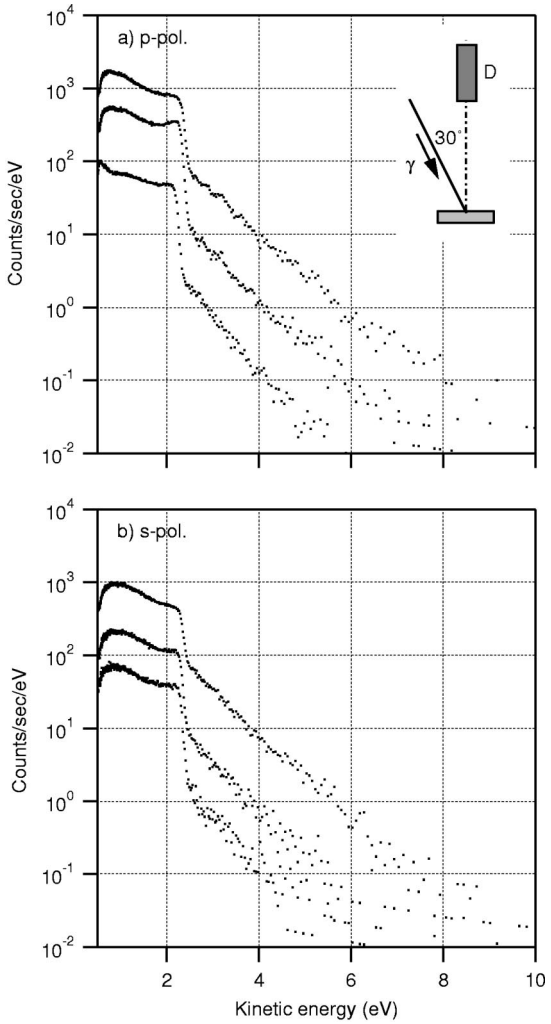

FIG. 4. Same condition of Fig. 3, except for the incidence angle which is now 30°. (a) Excitation with *p*-polarized light. (b) Excitation with *s*-polarized light.

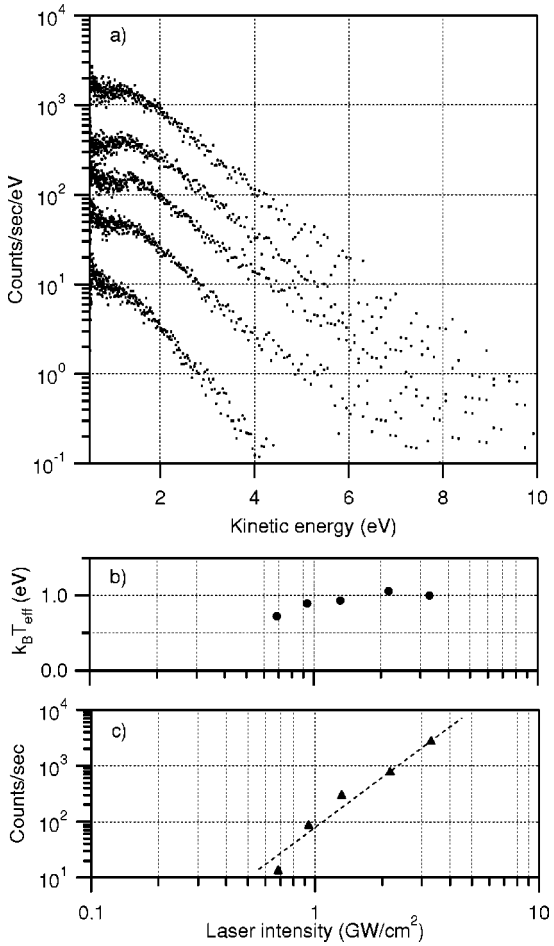

FIG. 5. Irradiation: $h\nu = 1.57$ eV, normal incidence (a) energy spectra of photoemitted electrons at different intensities. (b) Plot of the "effective temperature" (T_{eff}) versus intensity. Irradiated area: 1.1 mm^2. (c) Integrated electron yield versus intensity. Each point is obtained from the energy integration of the spectra reported in (a). The dashed line represents a third order power dependence on intensity.

$h\nu = 0.8$ eV. Two different exponential functions are used to fit the high energy part of the spectrum and two temperatures are reported in the figure.

D. Emission from image states

Ag(100) has a band structure with a gap in the projected bulk band structure. Image potential states are positioned within this gap, at 0.53 eV ($n=1$) and 0.16 eV ($n=2$) below the vacuum level and at about 3.90 eV ($n=1$) and 4.27 eV ($n=2$) above the Fermi level.[21] In the past these image states have been the subject of several studies mainly focused to elucidate the properties of electrons confined in two dimensions or to inquire about their lifetime.[6,7] Features associated with these states appear in the spectrum of the photoelectrons which are emitted normal to the [100] surface after having been excited with an adequate photon energy. Usually an angular resolved resonant[22] 2PPE configuration is used and, in agreement with the selection rules of the dipole transitions, they are observed only with *p*-polarized radiation. To measure the surface states features, we set the Ag(100) surface perpendicular to the TOF axis and tune the parametric oscillator so that its fourth harmonic provides a beam with photon energy adjustable around 4 eV. The results of a measurement are reported in Fig. 7.

Concluding this section, we note that all the data reported in the figures are obtained with sample No. 1. Measurements at 0.8 and 1.5 μm have been repeated with sample No. 2. We found no difference in the spectra, and hence no dependance of the data on the sample roughness.

IV. DISCUSSION

A. Absorption

The values of n_r, the refractive index, and of R, the reflectivity of a flat surface, given in the literature are reported in Table I. In the table we also report $R_{\min}$, the lower boundary of the reflectivity obtained from our measurement. R differs from $R_{\min}$ by a few per cent. The difference $R - R_{\min}$ includes the experimental uncertainty, side scattering (light

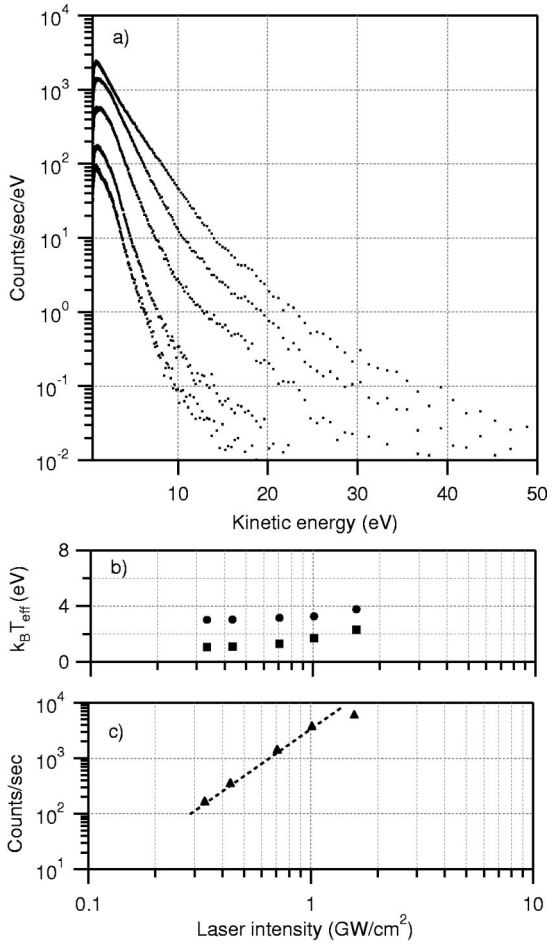

FIG. 6. Irradiation: $h\nu = 0.8$ eV, normal incidence (a) energy spectra of photoemitted electrons at different intensities. (b) Plot of the ''effective temperature'' (T_{eff}) versus intensity. The two temperatures represent the two different slopes clearly visible in the spectrum. (c) Integrated electron yield versus intensity. Each point is obtained from the energy integration of the spectra reported in (a). The dashed line represents a third order power dependence on intensity; Irradiated spot size 0.54 mm^2

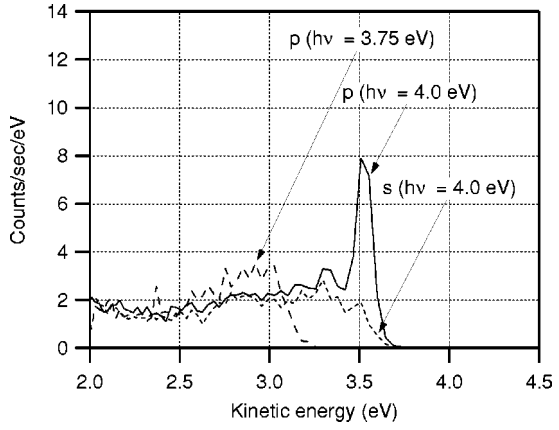

FIG. 7. 2PPE of the $n=1$ image state. Angle of incidence: 30°; Ag(100) surface perpendicular to the TOF axis. Polarization and photon energy as indicated.

TABLE I. Refractive index (n_r) and reflectivity (R).

	$h\nu = 3.14$ eV	$h\nu = 1.57$ eV	$h\nu = 0.8$ eV
n_r[a]	$0.17 - i1.95$	$0.14 - i5.2$	$0.45 - i8.5$
n_r[b]	$0.05 - i2$	$0.04 - i5.4$	$0.15 - i11$
R[c]	0.85	0.96	0.99
R[d]	0.86	0.98	0.98

[a]Ref. 23.
[b]Ref. 24.
[c]Ref. 25.
[d]Calculated using the refractive index in Ref. 23.

reflected outside the cone of collection) and ''extra absorption'' such as the one due to the coupling of the radiation to surface plasmons through roughness.

B. Image states

In Fig. 7, the sharp peak positioned around 4 eV is the signature of the $n=1$ image state. It disappears when the radiation is *s* polarized, in agreement with the selection rules of the dipole transitions, and when $h\nu < 3.9$ eV. The image states are confined along *z*, the direction normal to the surface, and the component of the wave function relative to this direction depends on the index *n*. Along the surface the electrons are free, they possess a translational energy $E_{\parallel} = \hbar^2 k_{\parallel}^2/2m$ ($k_{\parallel}$ is the momentum parallel to the surface) and, similarly to any two-dimensional gas, they can be divided into subbands, one for each *n*. The width of the peak in Fig. 7 arises from the instrumental resolution, the spectral width of the optical pulse, the dephasing time of the image states and the spread in energy of all the states which contribute to it. The latter spread depends on the spread of their $k_{\parallel}$'s. For a flat surface perpendicular to the detector axis the spread of $k_{\parallel}$'s depends only of the acceptance angle of the detector, but if the surface is locally tilted from normal, the spread depends on the magnitude of this random tilt. In fact, should an electron originate from a surface which is locally tilted 10 degrees from the normal, it would have a nonvanishing $k_{\parallel}$ and then a KE which is 0.15 eV larger with respect to the states at the bottom of the $n=1$ subband. The width of the experimental peak associated to the $n=1$ state in Fig. 7 is smaller than 100 meV and this shows that, at the microscopic level, the surface has an average tilt smaller than 10°.

C. Emission and spectrum

The most puzzling aspects are the electrons emitted with high kinetic energy and, when the exciting radiation is in the infrared, even the photoemission process itself. We shall analyze in the following some of the possible mechanisms.

1. Hot electrons and Coulomb repulsion

Hot electrons were first reported by Farkas *et al.*[12] in conjunction with 30 ps irradiation at $h\nu = 1.17$ eV. Reference 14 suggested that the high KE arose from the explosion of the photoemitted electron bunch due to Coulombic repulsion. Even if confuted in subsequent experiments,[15] the possibility

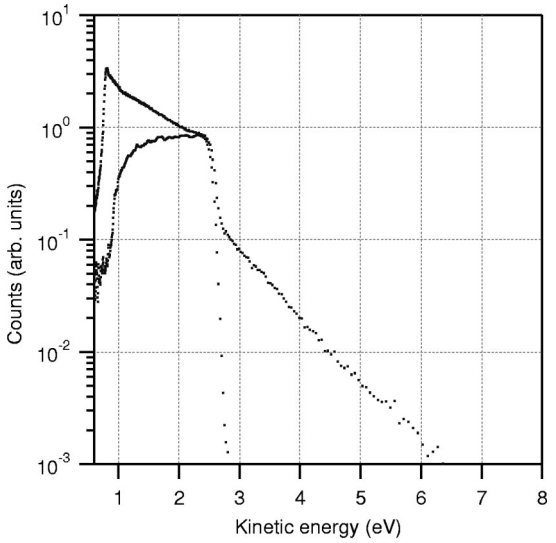

FIG. 8. Comparison of 1PPE and 2PPE spectra obtained with a similar count rate.

of such mechanism must be considered when irradiating with pulses since the electrons are emitted in a short bunch and the charge density can easily become rather high. In the present experiment, however, there is sufficient evidence to rule it out. In fact, we observe hot electrons also at low irradiation intensity and at yields smaller than 100 electrons/shot. An even more convincing argument against Coulombic explosion is offered by Fig. 8, where the spectra at $h\nu = 3.14$ eV and at 6.28 eV are both shown on a log scale. Hot electrons are absent in the case of linear emission ($h\nu = 6.28$ eV), in spite of the fact that the total count rate is about 3 times larger than at 3.14 eV.

2. Electron heating and thermal emission

The emission rate of thermal origin is evaluated with the Richardson equation using the electronic temperature induced by the laser pulses. The temperature of the electrons is calculated with the two-fluid model,[1,4] which assumes the system to be made by an electron gas in equilibrium within itself (this is justified by the short thermalization time among electrons) and by the lattice. The energy absorbed from the laser beam is deposited into the electrons of the metal (the region $z<0$) according to $e^{\nu^m z}$, with $1/\nu^m$ the penetration depth of the evanescent field in the metal. The energy is transferred locally from the electrons to the lattice accordingly to the magnitude of the coupling parameter g (see Table II), while each fluid through the respective thermal conductivities provides transport in a diffusion regime. The parameters adopted in the simulation are listed in Table II. In Fig. 9 we plot the predicted temperature at the surface versus the absorbed fluence. The energy transferred to the lattice during the laser pulse is negligible for any reasonable value of the coupling parameter g. The surface temperature T_s and the penetration depth $1/\nu^m$ are almost independent on the optical frequency. At $h\nu = 1.57$ eV, T_s reaches just 330 K when $I = 1$ GW/cm^2 and $1-R = 0.02$ (absorbed fluence $= 3$ mJ/cm^2). The small absorption of Ag, corroborated by its high thermal electronic conductivity, is the reason of the small increase of the temperature. As expected, the calculated thermal emission turns out to be negligible in most of the intensity range of the experiment and, on the other side, it cannot explain the high ''effective temperature'' of the spectrum. A better model could be represented by a very hot electron gas (with $T \approx T_{\text{eff}}$) produced by surface plasmons, limited to an area much smaller than the irradiated surface. This possibility will be discussed in Sec. V A.

TABLE II. Physical parameters of Ag at a wavelength of 395 nm.

λ: wavelength (nm)	395
R: reflectivity [a]	0.86
α: absorptivity [a] (m^{-1})	6.1×10^7
K: thermal conductivity [b] (W/mK)	419
C_l: lattice heat capacity [c] (J/m^{3}K)	2.6×10^6
γ: electronic heat capacity [d] (J/m^{3}K^2)	95
g: electron-phonon coupling [d] (W/m^{3}K)	10^6

[a]Ref. 23.
[b]Ref. 26.
[c]Ref. 27.
[d]Ref. 28.

3. Multiphoton emission

When the photon energy is less than the work function $h\nu < W$, the first mechanism to be considered for photoemission is a multiphoton process. The main features of multiphoton emission are the minimum number of photons n_{ph} for which $n_{\text{ph}} h\nu > W$, the maximum KE of the ejected electrons given by $\text{KE}_{\text{max}} = n_{\text{ph}} h\nu - W$, the yield of nPPE scales as $I^{n_{\text{ph}}}$, the intensity necessary to produce a given yield increases by orders of magnitude with n_{ph}. 2PPE measurements performed with $h\nu = 3.14$ eV exhibits all these fea-

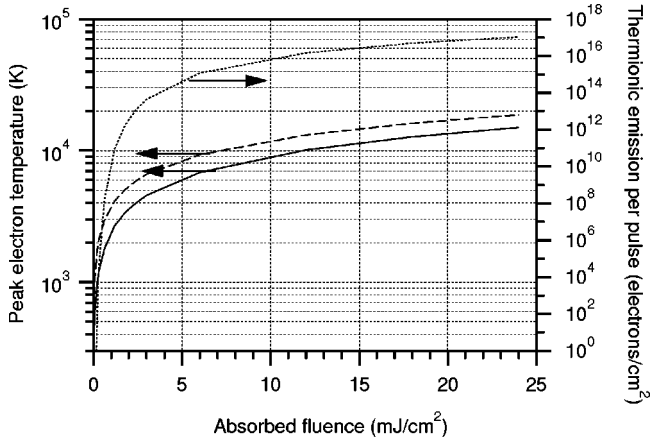

FIG. 9. Plot of the surface temperature (solid line) and of the consequent thermal emission (dotted line) versus the absorbed fluence, as calculated with the two-fluid model and the parameter of the simulation as in Table II. The dashed line represents the surface temperature calculated assuming no thermal conduction. Pulse duration 150 fs.

tures, and—when plotted versus $n_{ph}h\nu$—the spectra at $n_{ph}=1$ and $n_{ph}=2$ show the same cutoff at the Fermi edge (Fig. 8).

The interpretation is controversial at $h\nu=1.57$ eV. The yield scales as I^3, a fact that suggests a three-photon emission. However, with respect to the findings at $h\nu=3.14$ eV, a comparable yield occurs at intensities not much larger and there is no cutoff or discontinuities in the spectrum at energies corresponding to KE_{max} with $n_{ph}=3$ (or $n_{ph}=4$). Photoemission from metals ($W\approx 4-5$ eV) on irradiation at ≈ 1.5 eV has been usually attributed to a multiphoton process with $n_{ph}=3$ or 4, the order depending on the exact value of the work function and of the photon energy. This assignment is supported by the dependence of the yield on the third or on the fourth power of the intensity. The present results, in relation to the magnitude of the laser pulse intensity and the shape of the spectrum, question this interpretation, even if the strength of the argument may not be conclusive (for example, one could invoke temperature effects or consider that mechanism of electron acceleration subsequent to its emission could modify and smear the spectrum at 1.57 eV more effectively than at 3.14 eV).

The ambiguity of interpretation regarding the multiphoton origin of the photoemission disappears at $h\nu=0.8$ eV, where none of the features of multiphoton emission are observed. At this wavelength the dependence of the yield on intensity is close to a third power (see Fig. 6), which is certainly inconsistent with a multiphoton process which should be at least of sixth order.

4. Tunneling ionization

Tunneling ionization was proposed in Ref. 16 to explain the presence of high kinetic energy electrons in spectra obtained with $h\nu=1.6$ eV. In a tunneling process, the energy of the electrons depends on the phase and the amplitude of the field at the instant of emission and can results in a continuum spectrum. In the case of atoms the separation between the regime of multiphoton ionization and that of tunneling is controlled by the Keldysh parameter $\gamma=\sqrt{W_p/2U_q}$, where W_p is the ionization potential and $U_q=\frac{1}{4}mv_q^2$ is the ponderomotive potential, v_q the quiver velocity of the electron, given by $v_q=eE/m\omega$ with E the peak amplitude of the field and m is the electron mass. The parameter γ is usually used to separate the multiphoton mechanism ($\gamma\gg 1$) from the tunneling ($\gamma\ll 1$) regime. An estimation of the photoemission regime at a metal surface can be done by applying the same relations. Given $h\nu=1.57$ eV, $W=4.5$ eV, $E=10^8$ V/m (the corresponding intensity in vacuum is $I=1.5$ GW/cm^2), it results $U_q=5\times 10^{-5}$ eV and $\gamma=250$. Fields ≈ 300 times larger are then necessary to promote tunneling. Such fields—when the ponderomotive potential is converted to kinetic energy and the effect of the phase is taken into account—would accelerate the electrons to $KE\approx 2U_q\approx 10$ eV. It results that emission of hot electrons can only be accounted for by fields much larger than those associated with the impinging pulse in our experiment. Aeshlimann and co-workers invoked to this end surface plasmons (SP) and suggested surface roughness as the coupling mechanism for their excitation.[16]

Electrons with high kinetic energy have been recently reported with arrangements specifically designed to couple the laser pulse to surface plasmons.[17,18] Such arrangements are based on a grating which modulates the surface depth or on a Kretchmann geometry (total internal reflection at a prism-metal film interface). As expected, both experiments show a crucial dependence of the yield on the angle of incidence, a clear sign that the laser field is being coupled to surface plasmons. Back to our case, however, the question is whether and how the modest ripples of the nominally flat surface of our sample can provide the excitation of SP up to a 10^3 increase of the field.

We conclude this section with the following summary: by decreasing the photon energy and increasing the intensity the photoemission moves from a 1PPE to a 2PPE regime, as expected. On a further decrease of $h\nu$, it is not observed the nPPE of higher order, since before reaching the necessary intensities another mechanism of photoemission sets in. The two different physical processes are simultaneously present on irradiation with 3 eV photons. The new mechanism of photoemission could be explained by conventional processes if the fields were much larger than those associate at the laser pulses at the intensities considered in these experiments. As in other context of surface physics, the enhancement mechanism based on surface plasmons and surface roughness can be invoked to this end. The question is whether there is matter to accept it and whether there is some independent evidence in favor or against it. This question is the topic of the next section.

V. SURFACE PLASMONS AND SURFACE ROUGHNESS

The aim of this section is to comment on the role of surface plasmons associated to surface roughness and establish whether it is worth to push further the investigation in this direction or whether, as we believe, they are not the crucial elements which can explain the anomalous hot electrons in the spectrum. It is probably worth saying that evidences are not always clear cut or definitively conclusive, as often occurs when random features—such as roughness in this case—are involved. We shall first summarize and discuss the magnitude of field enhancement promoted by SP. In the second part we comment on a possible explanation based on SP, either because they promote tunneling and acceleration or because they promote in a few spots a strong electron heating.

A. Field enhancement by surface plasmons

To describe surface plasmons it is common practice to use a different approach according to the level of scattering and, ultimately, of the surface roughness. SP which propagate on a fairly flat surface, with a scattering that can be treated as a perturbation, are called PSP's (propagating surface plasmons). When the roughness of the surface becomes large, the scattering increases and it cannot be treated just as a perturbation. Plasmon localization is likely to occur, and one talks of LSP's (localized surface plasmons).

1. Propagating surface plasmons

We briefly recall the properties of PSP on an ideal metal surface. Assuming a sharp discontinuity at $z=0$ between the metal ($z<0$, relative dielectric constant ε_m) and the the vacuum ($z>0$, $\varepsilon_v=1$), the SP field can be written as

$$\mathbf{E}_{\mathrm{SP}}=\sum_{\mathbf{q}} A_q \mathbf{L}_{\mathbf{q}} e^{i(\mathbf{q}\boldsymbol{\rho}-\omega_q t)}, \tag{1}$$

where A_q is the amplitude of mode $\mathbf{q}$. The direction of the field and the mode profile along z are given by

$$\mathbf{L}_{\mathbf{q}}(z)=\begin{cases}\left(\mathbf{q}+\dfrac{iq}{\nu_q^m}\mathbf{z}\right)e^{\nu_q^m z} & \text{for } z<0,\\ \left(\mathbf{q}+\dfrac{iq}{\nu_q^v}\mathbf{z}\right)e^{-\nu_q^v z} & \text{for } z>0,\end{cases}$$

where $\mathbf{z}$ is a unit vector along the z axis and

$$(\nu_q^m)^2=q^2-\varepsilon_m\omega_q^2/c^2,$$

$$(\nu_q^v)^2=q^2-\varepsilon_v\omega_q^2/c^2,$$

$$\varepsilon_m/\nu_q^m=\varepsilon_v/\nu_q^v.$$

For large q, ω_q levels off at $\tilde{\omega}\simeq 3.6$ eV in Ag, while at small q's, q is close to but always somewhat larger than ω_q/c. Making use of the refractive index of Ref. 23, we calculate that, at $h\nu=1.5$ eV, the SP field extends up to $1/\nu^m \approx 500$ nm from the surface in the vacuum side and, similarly to the laser field, to a depth $1/\nu^v \approx 20$ nm in the metal. Its z component, which accounts for the major part of the energy of the SP, decreases by a factor 25 on crossing the vacuum-metal interface. Assume the laser beam to be normal to the surface, with the impinging field given by $\mathbf{E}_{L,in}=\mathrm{Re}\{\mathbf{E}_L e^{i(kz-\omega t)}\}$. Due to the large reflection it forms an almost standing wave in vacuum, with an amplitude $\approx 2E_L$ at 0.4 μm from the surface and $\approx 0.15E_L$ at the surface. Direct coupling of the laser field with surface plasmons is not allowed since momentum conservation is not satisfied, but it can occur through surface roughness. The strength of the coupling with a plasmon of wave vector q is proportional to h_q, the fourier transform of the roughness height. One can estimate the amplitude of A_q by making use of the AFM data on h_q. The power spectrum is rather flat, with A lorentian shape that changes smoothly in the region of interest (the range of q's with ω_q in resonance with the various frequencies of irradiation) so that coupling to PSP can take place at every photon energy. An estimate of the maximum plasmon energy can be quickly made from absorption. At $h\nu=1.57$ eV, attributing the whole difference between R and $R_{\min}$ to A_{sp}, the absorption of surface plasmon, we derive from Table I: $A_{\mathrm{SP}}=R-R_{\min}=0.03$ (we stress that this is just the upper limit). At this wavelength the component of the field normal to the surface in the vacuum side accounts for almost all the energy of the surface plasmon, whose energy per unit area can be expressed as $w_{\mathrm{SP}}=(1/2)\varepsilon_0\langle|\mathbf{E}_{\mathrm{SP}}^v|^2\rangle(2\nu^v)^{-1}$, where $|\mathbf{E}_{\mathrm{SP}}^v|$ is the amplitude of the SP field just at the vacuum-metal discontinuity. Setting w_{SP} equal to the absorbed laser fluence, given by $(1/2)\varepsilon_0 c|\mathbf{E}_L|^2 A_{\mathrm{abs}}\tau_p$ (τ_p is the pulse duration), the root mean square (r.m.s.) value of the plasmon field compared to the exciting laser field is

$$E_{\mathrm{SP}}^v/E_L \approx \sqrt{A_{\mathrm{abs}} c\tau_p (2\nu^v)}. \tag{2}$$

This result is quite intuitive when considering that $c\tau_p$ represents the pulse length l_p. We have neglected plasmon damping, an assumption quite reasonable since the resonance factor is larger than 100, exceeding the number of optical cycles in the laser pulse. Substituting the appropriate values one obtains, at $h\nu=1.57$ eV, $E_{\mathrm{SP}}^{(v)}\approx 2E_L$. The r.m.s. amplitude of the SP field at the surface is then comparable to the laser field. But locally the SP field can be much larger, this depending on the phases of the $\mathbf{q}$ components which enter in the summation of Eq. (2). During their lifetime the plasmon propagates for a length ≈ 100 μm. If all the energy of the plasmon wave which is contained in an area of 100×100 $\mu\mathrm{m}^2$ could be made to collapse into a spot of size λ^2, one would have a local field enhancement of 100. The unique possibility of concentrating the energy of an ultrafast excitation of a nanosystem in a small part of the whole system by means of coherent control has been put forward very recently.[29] The effect is based on phase modulation of the exciting ultrashort pulse and on the propagation properties of surface plasmons. For an engineered system with an appropriate geometry and an excitation pulse with a tailored phase profile, the authors calculate a field enhancement as large as 100. A similar effect should exist to some extend also for a random system and a pulse with a residual chirp, but the maximum conceivable enhancement is certainly much smaller.

2. Localized surface plasmons

Field enhancement by LSP has been studied in relation to surface enhanced Raman scattering.[30–33] Prepared by vapor deposition, the Ag surfaces can be made rough or smooth according to the substrate temperature and the subsequent annealing. The rough surfaces which promote a large enhancement are made by clusters, typically 10–100 nm in diameter and separated among each other by a distance of 2–3 diameters. Raman enhancement as high as 10^5-10^6 have been reported, which suggest that the field has peaks which are larger by a factor 20–30 than the average. A similar 20-fold increase has been estimated from the enhancement of the SH observed by moving from a smooth Ag surface to a rough one. The rough surface was fabricated by electrolytic cycling and consisted of spheroids, about 50 nm in diameter, covering 5% of the whole area.[31]. Following Mc Call *et al.*,[32] rough Ag surfaces prepared on purpose are better modelled by an ensemble of independent spheres than by an approach based on the ''roughness.'' At the surface of a small metallic spheres (with diameter sufficiently small so that $d\ll\lambda$) the field scales according to $\varepsilon_m-1/\varepsilon_m+2$. Close

to the resonant frequency—attained at $\varepsilon_m+2\approx 0$—the enhancement scales approximately as $3/\mathrm{Im}(\varepsilon_m)$. The more accurate calculations of Ref. 33 show that the largest field enhancement (≈ 30) occurs for spheres of 10 nm size and photon energy around 3.2 eV. The enhancement decreases to 6 and moves to longer wavelength for 100 nm spheres, decreasing further for those of 1000 nm size.

Summarizing, we conclude that local field enhancements up to 20–30 times the laser field are conceivable in surfaces specifically prepared for this purpose. From the models proposed it does not seem possible that such enhancements can take place at all the wavelengths, as it would be necessary to justify our results. The surfaces to which such large enhancements refer are quite different in terms of roughness from the monocrystal used in our measurements and have been specifically prepared.

B. Are surface plasmons involved?

SP can give rise to tunneling photoemission and to electron acceleration up to the observed KE. However, as presented in Sec. III, field enhancement of a few hundreds are needed to this end. As discussed above, this figure is larger than conceivable in the best engineered situations. SP do not really seem to be involved since one would expected some difference in the spectrum on changing from sample No. 1 to sample No. 2, this in view of the different coupling promoted by the roughness.

Concerning LSP, consider an extreme scenario where a 30–40-fold field enhancement takes place in hot spots of very small size. In this situation, it is possible to reach a surface electron temperature $T_s\approx 0.5$ eV at $h\nu=1.57$ eV with a laser intensity of 1 GW/cm^2. The thermal emission rate at this temperature is about 10^4 particles/μm^2. LSP localized around nanostructures of 100 nm size, with density 10^4 cm^{-2}, could bring to such an emission rate. In the case of Figs. 3 and 4, 2PPE would come from the whole 1 mm^2 cold surface while hot electrons production would be limited to the 1 μm^2 surface with high electron temperature. It should be noticed that with such a ratio between the two areas, 2PPE from hot spots is negligible even taking into account the larger local field and the dependence of 2PPE on I^2. Excitation of LSP in the IR should also be more difficult than at 3 eV, a fact that is not evident in the photoemission yield. We notice that an extended nanoroughness can be ruled out from the experimental results. In fact, being a nonlinear process, resonant 2PPE is expected to occur preferentially where the field is the largest and hence around the localized roughnesses, if present. But emission from a spheroid, or from a curved surface would be contradictory with the narrow energy peak of the image state in Fig. 7. Valuable information to this regard could come from a more detailed analysis and further data at low KE. In fact, in their interpretation of 2PPE from Ag films, the authors of Ref. 34 argue that, in addition to the direct transitions, the strongly inhomogeneous field of LSP promotes indirect transitions. The signature of the latter is the ''rectangular 2PPE spectra'' that these authors observe with rough surfaces.

We would like to mention that photoemission from a gold sample under irradiation of midinfrared pulses at very small intensity has been found by Farkas and collaborators.[35] A tail of high KE in the electron distribution and the consequent emission has been attributed by the authors to the peculiar condition one obtains when the collision time is close to the half cycle of the em field. A further validation of this model has been recently reported.[36] However, we notice that the specific condition of the model are far from being met in any of the cases we considered in present experiment

VI. CONCLUSIONS

We have investigated the linear and the nonlinear photoemission from a silver monocrystal under short pulse irradiation. Decreasing the photon energy from 6.28 to 3.14 eV and increasing the intensity, the photoemission changes, as expected, from the one-photon to the two-photon regime. In this regime the spectrum shows the appearance of an exponential distribution of high kinetic energy electrons on top of the 2PPE Fermi edge. At lower optical frequencies ($h\nu=1.57$ and 0.8 eV) this mechanism accounts for all the photoemission, the spectrum bearing no traces of a multiphoton process.

The present data unambiguously show that a multiphoton photoemission of third or fourth order has no chance to come into play since a masking process sets in at lower intensity. This new mechanism, which produces electrons with kinetic energies up to tens of eV, can be explained by conventional processes only if the optical fields at the surface are much larger than the nominal one of the laser. To this end we considered the chances of field enhancement through surface plasmons and surface roughness. Within this frame, a possible scenario consists of photoemission of thermal nature from relatively few hot spots, these being made by protrusions or roughnesses of nanometer size heated by localized surface plasmons. The problem, however, is open to more satisfactory interpretations.

However speculative, the picture of a tiny fraction of electrons, heated by the laser and decoupled from the majority in the background at lower energy, is certainly suggestive. Surface effects, and the 2D gas of the image states can be considered to this end. Other mechanism we believe worth investigating are multielectron processes, whereby the energy of two or more particles is added for a larger energy of a single one.

ACKNOWLEDGMENTS

The authors would like to thank M. Lazzarino and B. Ressel for kindly providing us the AFM data of the two samples. We acknowledge the support of the Istituto Nazionale Fisica della Materia (PRA Elphos) and of the Ministero della Università e della Ricerca.

[1] S.I. Anisimov, V.A. Benderski, and G. Farkas, Sov. Phys. Usp. **20**, 467 (1977).
[2] J.H. Bechtel, W.L. Smith, and N. Bloembergen, Phys. Rev. B **15**, 4557 (1977).
[3] R. Yen, J. Liu, and N. Bloembergen, Opt. Commun. **35**, 277 (1980).
[4] J.G. Fujimoto, E.P. Ippen, J.M. Liu, and N. Bloembergen, Phys. Rev. Lett. **53**, 1837 (1984).
[5] P.M. Echenique and J.B. Pendry, Prog. Surf. Sci. **32**, 111 (1990).
[6] R. Haight, Surf. Sci. Rep. **275**, 21 (1995).
[7] R. M. Osgood Jr. and X. Wang, *Solid State Physics* (Academic, San Diego, 1997), Vol. 51.
[8] H. Petek and S. Ogawa, Prog. Surf. Sci. **56**, 239 (1997).
[9] M. Bauer, S. Pawlik, and M. Aeschlimann, Phys. Rev. B **60**, 5016 (1999).
[10] A. Hotzel, M. Wolf, and J.P. Gauyacq, J. Phys. Chem. B **104**, 8438 (2000).
[11] H. Petek, H. Nagano, M.J. Weida, and S. Ogawa, J. Phys. Chem. B **105**, 6767 (2001).
[12] G. Farkas and C. Toth, Phys. Rev. A **41**, 4123 (1990).
[13] C. Toth, G. Farkas, and L.K. Vadopyanov, Appl. Phys. B: Photophys. Laser Chem. **53**, 221 (1991).
[14] G. Petite, P. Agostini, R. Trainham, E. Mevel, and P. Martin, Phys. Rev. B **45**, 12 210 (1992).
[15] G. Farkas, Cs. Toth, and A. Kohazikis, Opt. Eng. (Bellingham) **32**, 2476 (1993).
[16] M. Aeschlimann, C.A. Schmuttenmaer, H.E. Elsayed-Ali, R.J.D. Miller, J. Cao, Y. Gao, and D.A. Mantell, J. Chem. Phys. **102**, 8606 (1995).
[17] J. Zawadzka, D.A. Jaroszynski, J.J. Carey, and K. Wynne, Appl. Phys. Lett. **79**, 2130 (2001).
[18] M.R.J. Kupersztych and P. Monchicourt, Phys. Rev. Lett. **86**, 5180 (2001).
[19] J.P. Girardeau-Montaut and C. Girardeau-Montaut, J. Appl. Phys. **65**, 2889 (1989).
[20] S. Varro and F. Ehlotzky, J. Phys. D **30**, 3071 (1997).
[21] K. Giesen, F. Hage, F.J. Himpsel, H.J. Reiss, and W. Steinmann, Phys. Rev. B **35**, 971 (1987).
[22] Resonant because the intermediate state is accessed with a real transition, the first photon populates the image state while the second ionizes it.
[23] D. W. Lynch and W. R. Hunter, *Handbook of Optical Constants of Solids* (Academic, Orlando, 1985).
[24] P.B. Johnson and R.W. Christy, Phys. Rev. B **6**, 4370 (1972).
[25] J. H. Weaver, C. Krafka, D. W. Lynch, and E. E. Koch, *Optical Properties of Metals*, Vol. 18-1/2 of *Physics Data* (Fachinformationszentrum, Karlsruhe, 1981).
[26] *Metals Reference Book*, edited by C. J. Smithells (Butterworth, London, 1976).
[27] N. W. Ashcroft and N. D. Mermin, *Solid State Physics* (Saunders, Philadelphia, 1988).
[28] S.D. Brorson, A. Kazeroonian, J.S. Moodera, D.W. Face, T.K. Cheng, E.P. Ippen, M.S. Dresselhaus, and G. Dresselhaus, Phys. Rev. Lett. **64**, 2172 (1990).
[29] M.I. Stockman, S.V. Faleev, and D.J. Bergman, Phys. Rev. Lett. **88**, 067402 (2002).
[30] T. Vo-Dinh, *Surface Enhanced Raman Scattering, Photonic Probes of Surfaces* (Elsevier Science, British Vancouver, 1995).
[31] C.K. Chen, A.R.B. de Castro, and Y.R. Shen, Phys. Rev. Lett. **46**, 145 (1981).
[32] S.L. Mc Call, P.M. Platzman, and P.A. Wolf, Phys. Lett. **70A**, 381 (1980).
[33] M. Kerker, Acc. Chem. Res. **17**, 271 (1984).
[34] C. Douketis, T.L. Haslett, J.T. Stuckless, M. Moskowits, and V. Shalaev, Surf. Sci. **297**, L84 (1993).
[35] G. Farkas, C. Toth, A. Kohazi-Kis, P. Agostini, G. Petite, P. Martin, J.M. Berset, and J.M. Ortega, J. Phys. B **31**, L461 (1998).
[36] F. Pisani, J.L. Fabre, S. Guizard, P. Palianov, P. Martin, F. Glotin, and J.M. Ortega, Phys. Rev. Lett. **87**, 187403 (2001).